INTERNATIONAL JOURNAL FOR NUMERICAL AND ANALYTICAL METHODS IN GEOMECHANICS, VOL. 21, 91–120 (1997)

TWO-PHASE OIL MIGRATION IN COMPACTING SEDIMENTARY BASINS MODELLED BY THE FINITE ELEMENT METHOD

MAGNUS WANGEN

Institutt for Energiteknikk, Box 40 N-2007 Kjeller, Norway

SUMMARY

The upstream-weighted finite element method with lumped mass matrix is applied to the modelling of oil migration in compacting sedimentary basins. An implicit formulation is made in Lagrangian co-ordinates of a pressure, saturation and a temperature equation, which is based on immiscible two-phase flow of oil and water. The formulation accounts for the compaction of the sediments, the generation of oil from solid organic material (kerogen), the eventual pore space generated by kerogen breakdown, and the density variations of the fluids which may set up thermal convection. The model is validated by comparison with results from a one-dimensional (1D) fractional flow-based migration model. A 2D case example showing oil expulsion from source rocks, and the filling of a trap is presented. The mass balance of the model is easily checked because all oil in the basin originates from breakdown of kerogen. Compared with other alternatives, the simple upstream-weighted finite element method is suggested as a possible first choice for a numerical method for the modelling of oil migration in compacting sedimentary basins. It easily deals with the complex geometry of a basin, it yields reasonably good results, is simple to implement, and the same implementation applies to all spatial dimensions. © 1997 by John Wiley & Sons, Ltd.

Int. j. numer. methods geomech., vol. 21, 91–120 (1997)
(No. of Figures: 10 No. of Tables: 8 No. of Refs: 41)

Key words: finite elements; oil migration; immiscible two-phase flow; compaction

1. INTRODUCTION

Migration of hydrocarbons in sedimentary basins is usually divided into two parts: primary migration, which is the movement of the hydrocarbons inside the source rock where they are formed, and secondary migration, which is the subsequent migration outside the source rock. The hydrocarbons may migrate over long distances, during secondary migration, if they reach permeable carrier beds. Parts of the hydrocarbons may also be trapped in reservoirs formed by for instance anticlinals or fault zones (see Reference 1).

The formation and migration of hydrocarbons in sedimentary basins through geological time is intimately connected to the formation of the basin. This is a complex process that includes the deposition of different lithologies at different rates, erosion processes, fracturing and faulting due to for instance tectonic stresses, diagenesis, ingeous intrusions and salt movements.

In this paper the focus is restricted to a numerical implementation of a finite element method for study of the migration process. It accounts for the compaction of the sediments, and changes in basin geometry.

CCC 0363–9061/97/020091–30

Received 5 June 1995
Revised 6 June 1996

The dimensions of the time scale, which may be of the order 100 Ma (Ma = 10^6 y), make this kind of modelling computationally demanding for high fluid flow rates. The Courant–Friedrich–Levy (CFL) condition, which constrains the time step for explicit methods, will often produce reasonable time steps owing to the large dimensions of the basins. Sedimentary basins are typically a few km deep, and a few tens of km wide. Nevertheless, grid refinement in permeable parts of a basin may easily lead to large computing times.

The model reduces to single-phase flow in a compacting sedimentary basin in absence of oil. There exist several numerical models which study the pressure and the temperature development in this case, see for instance, References 2–12.

Oil migration has been modelled for at least 20 years, where the best-known model is probably the commercially available simulator Themis, made by Institut Francais du Petrole (IFP).[13] This is a two-phase compositional simulator, which has been used in studies of several basins and oil provinces,[13] and it is based on a Finite Volume Method (FVM). Other models for oil migration, like Faille[14] and Schneider *et al.*,[15] are also based on the FVM. A numerical model of oil migration based on the finite difference method is presented by Wendebourg.[16]

The FVM is often implemented as a cell-centred method, as done by Faille[14] and Schneider *et al.*[15] However, the mass flux at the cell interfaces, which is an important part of the FVM, is less trivial to calculate for irregular cell-centred grids. This is owing to the gradient operator, which is not straightforward to discretize for irregular cell centre positions in 2D and 3D; see, for instance, References 14 and 17.

There exist several Finite Element Methods (FEM) applied to two-phase flow in porous media, for instance the stream line diffusion FEM[18] and the characteristic based FEM.[19,20] The one selected here for the modelling of oil migration is the simple upstream-weighted FEM with lumped mass matrix proposed by Dalen,[21] Huyakorn and Pinder,[22] Khataniar and Ekwere,[23] Langsrund,[24] and Spivak *et al.*,[25] among others. This FEM is reported to produce the same solutions as the standard finite difference methods of reservoir engineering; see References 23 and 26.

The upstream-weighted FEM with mass-lumping is straightforward to implement. Furthermore, once implemented, the FE-formulation applies equally well in any spatial dimension. The FEM considered here is implicit. Hence, it is more stable and robust, and allows for larger time steps than its explicit versions, but at the price of more computational work per time step. However, there is not normally oil everywhere in a basin, and an explicit method may therefore be a simple mean of reducing the computational burden to the limited parts of the basin where oil is found.

This paper is organized as follows, by first presenting the assumptions used for sedimentary rocks and then presenting the physical model and then the numerical implementation. The numerical model is validated by comparison with the results of a 1D migration model based on a fractional flow formulation, before a 2D case example is given.

2. DEFINITIONS AND ASSUMPTIONS

2.1. Rock description and co-ordinate spaces

The rock considered here is assumed to consist of three basic parts: Rock without any hydrocarbon potential, pure kerogen where all the kerogen may be broken down to oil, and a void part initially filled with water. The height of a sediment grain from the basement measured as compacted rock without any kerogen, ζ, is chosen as the Lagrangian co-ordinate in the migration model (see References 27 and 28). The ζ-co-ordinate is neither influenced by the

compaction of the sediments, nor by the fact that a part of the solid sediment skeleton is transformed to a hydrocarbon fluid. The z-position of ζ-particle is given by (see Reference 28 for a derivation)

$$z(x, y, \zeta) = -\int_{\zeta}^{\zeta^*(t,x,y)} \frac{(1 - C_0 + C(x, y, \zeta'))}{(1 - C_0)(1 - \phi(x, y, \zeta'))}\, \mathrm{d}\zeta' + a(x, t)(t, y, y) \tag{1}$$

where the height of the basin along the ζ-axis is denoted ζ^*, and z_0 is the water depth down to the basin surface. The total kerogen content, denoted C, is given as a volume fraction of the initial solid rock matrix, (see Reference 28), and C_0 is the initial kerogen constant. The porosity is ϕ. A minus sign is added to the integral equation (1), because $z = 0$ is defined to be the water surface above the basin. From equation (1) it is seen that the basin bottom is given by $\zeta = 0$. The lateral position of the sediment grains is constant during the compaction process, thus the model considers vertical compaction only. Both the z-axis and the ζ-axis are pointing upwards. The transformation between the x–y–ζ and the x–y–z-spaces, defined by (1), gives rise to the Jacobian of the form

$$\mathbf{J}(x', y', \zeta) = \frac{\partial(x, y, z)}{\partial(x', y', \zeta)} = \begin{pmatrix} 1 & 0 & \dfrac{\partial z}{\partial x} \\ 0 & 1 & \dfrac{\partial z}{\partial x'} \\ 0 & 0 & \dfrac{(1 - C_0 + C)}{(1 - C_0)(1 - \phi)} \end{pmatrix} \tag{2}$$

where the determinant $|\mathbf{J}|$ is

$$|\mathbf{J}| = \frac{f(C)}{(1 - \phi)} \tag{3}$$

and where $f(C) = 1 + C/(1 - C_0)$. Notice that the matrix elements $\partial z/\partial x'$ and $\partial z/\partial y'$ do not appear in the determinant $|\mathbf{J}|$. It should be noted that $f(C) = 1$ outside source rocks because $C = 0$ there. The initial kerogen content is likely to be small inside the source rocks, since $C_0 < 0{\cdot}05$, and f is therefore close to one, $f \approx 1$.

2.2. *Kerogen breakdown to oil*

The kerogen is assumed to be composed of several groups, which decay with their own reaction rates. The total kerogen content C is related to the content of each group C_i by $C = \sum_i^N C_i$, where N is the number of groups. The kerogen concentration of group i, C_i, is defined in the same way as C, as a volume fraction of the initial solid part of a rock sample. The kerogen breakdown is given by a set of parallel first-order reactions of the Arrhenius-type:

$$\frac{\mathrm{d}C_i}{\mathrm{d}t} = -k_i C_i \tag{4}$$

where

$$k_i = A_i \exp(-E_i/RT) \tag{5}$$

see Reference 35. The constants defining the reaction rate k_i are the prefactor (Arrhenius factor) A_i, the activation energy E_i, the gas constant R, and the temperature T (K).

2.3. Pressure definitions

The compaction of the sediments in response to the increase in load caused by deposition of new sediments is assumed to be vertical, as expressed by equation (1). Furthermore, the porosity or the compaction is assumed to be given by empirical functions of the effective stress in the vertical direction, which is the usual approach to fluid flow and compaction modelling in sedimentary basins, see References 2, 4, 8–11 and 32. The vertical effective stress denote σ_e, is defined as

$$\sigma_e = \sigma_T - p_f \tag{6}$$

which is the bulk pressure σ_T minus the fluid pressure p_f.

The fluid pressure is defined as a mean over the oil pressure p_o and the water pressure p_w, where each pressure is given weight proportional to their saturations, S_o and $S_w = 1 - S_o$,[29]

$$p_f = S_o p_o + S_w p_w \tag{7}$$

The bulk pressure at depth z is defined as

$$\sigma_T = \int_z^{z_0} [(1-\phi)\rho_m + \phi\rho_f]g \, dz + \int_{z_0}^{0} \rho_w g \, dz \tag{8}$$

which is the pressure due to the weight of the sediments and the pore fluids. Note that the constant of gravity g is positive, while the z-axis is positive upwards. The density of the rock matrix is denoted ρ_m. The fluid density ρ_f is defined as the mean of the oil and water densities, where the weight of each density is proportional to its saturation.

$$\rho_f = S_o \rho_o + S_w \rho_w \tag{9}$$

The average fluid pressure and the fluid density, given by the relations (7) and (9), are only needed in the computation of the effective stress.

The excess pressures of both oil and water $p_{i,e}$, $i = o, w$, are defined as the respective pressure minus the respective hydrostatic pressure

$$p_{i,e} = p_{i,w} - p_{i,h}, \quad i = o, w \tag{10}$$

The hydrostatic pressures $p_{i,h}$ are given by

$$p_{i,h} = \int_z^0 \rho_i g \, dz, \quad i = o, w \tag{11}$$

The difference between the oil pressure and the water pressure is the capillary pressure

$$p_c = p_o - p_w \tag{12}$$

which is assumed to be a given function of the oil saturation: $p_c = p_c(S_o)$.

2.4. Porosity as function of effective stress

The porosity is assumed to be a function of the effective stress, and the following empirical porosity function is assumed in this study:

$$\phi = \phi_0 \exp(-\alpha\sigma_e) \tag{13}$$

where ϕ_0 is the surface porosity and $1/\alpha$ is a characteristic pressure.[30] A similar relationship was suggested by Smith[8] on basis of the empirical porosity–depth relationship $\phi = \phi_0 \exp(-cz)$, found by Athy,[31] where the parameters ϕ_0 and c were fitted to well observations.

Another porosity function similar to (13), $e = (e_0 - e_\infty)\exp(-\alpha\sigma_e) + \sigma_\infty$, was suggested by Gibson *et al.*[32] for the consolidation of clays. The parameters e_0 and e_∞ are the surface void ratio and the void ratio at infinite effective stress, respectively. However, the relation which is usually applied to the consolidation of clays is

$$e = e_0 - C\log(\sigma_e/\sigma_{e,0}) \tag{14}$$

where the parameters e_0, C and $\sigma_{e,0}$ can be obtained from oedometer tests, see Reference 33.

The porosity development in sedimentary rocks through geological time is a complex process which is far from fully understood. It involves mechanical compaction by means of reorientation of the grains, together with cleavage and fracturing of the grains. The prorosity in sedimentary rocks is also influenced by mineral precipitation and dissolution. An empirical relation like (13) represents the combined effect of mechanical and chemical porosity changes. The empirical porosity function (13) is therefore assumed, because it yields porosity–depths trends in accordance with those first observed by Athy and later supported by several other authors.[1,34]

The compaction process is only slightly reversible, which implies that the porosity does not return to the earlier values if the effective stress is decreasing. This slight reversibility is simply accounted for by linear swelling

$$\phi = \phi_{\min}(1 + \alpha_e(\sigma_{s,\max} - \sigma_e)) \tag{15}$$

where $\sigma_{s,\max}$ is the maximal effective stress, and $\phi_{\min} = \phi(\sigma_{s,\max})$ is the associated minimal porosity. The new 'expansibility' α_e is chosen to be $\alpha_e = 1 \times 10^{-12}\ \mathrm{Pa}^{-1}$, which corresponds to the elastic modulus of consolidated sediments as quartz and shales. Note that the selected value for α_e is less than the compressibility of water.

2.5. *A porosity function for the source rocks*

The kerogen breakdown is likely to lead to an increase in the porosity of the source rock. Such an increase in porosity can be accounted for in the porosity relationship (13) by replacing the initial porosity ϕ_0 by

$$\phi = \phi_0 + (1 - \phi_0)(C_0 - C) \tag{16}$$

which is the porosity increase caused by kerogen breakdown in the case of no compaction (see Reference 28). The porosity function in presence of kerogen is then

$$\phi = (\phi_0 + (1 - \phi_0)(C_0 - C)\exp(-\alpha\sigma_\alpha) \tag{17}$$

It should be noted that morphological changes to the pores space in response to kerogen breakdown are poorly understood.

2.6. *Absolute permeability and thermal conductivity*

Both the absolute permeability $\mathbf{K} = \mathbf{K}(\phi)$ and thermal conductivity $\mathbf{L} = \mathbf{L}(\phi)$ are tensors, which are given as functions of the porosity. These porosity relationship provide a decreasing permeability and an increasing bulk heat conductivity during compaction of a layer. Both these

tensors are obtained by rotating their representations in the principal system to the real co-ordinate system. The principal system of a FE is defined by the lower lateral fact of the element (Reference 11 for details).

The permeabilities in the principal directions are

$$\mathbf{K} = \mathbf{diag}(K_1(\phi), K_2(\phi), K_3(\phi)) \tag{18}$$

where the scalar permeabilities $K_1(\phi)$, $K_2(\phi)$, and $K_3(\phi)$ in the three spatial directions are assumed to be of the form

$$K(\phi) = k_1 \exp(k_2 \phi) \tag{19}$$

suggested by Bryant *et al.*[36] (see Reference 3, where k_1 and k_2 are fitted to various lithologies).

The scalar anisotropic bulk thermal conductivities in the principal directions are of the form

$$\lambda(\phi) = \lambda_s^{1-\phi}(S_o\lambda_o + S_w\lambda_w)^{\phi} \tag{20}$$

where λ_s and $S_o\lambda_o + S_w\lambda_w$ denote the thermal conductivity of the sediment matrix and the fluid, respectively. This is a straightforward generalization of the bulk thermal conductivity suggested by Lewis and Rose[37] for single-phase flow. This is, however, a simple relationship, which ignores the temperature dependence of the heat conductivities.

2.7. *Relative permeability and capillary pressure*

The relative permeabilities of each phase are assumed to be given as power functions of the respective saturations, because these curves can be fit to most experimental data (see Reference 38)

$$k_{r,i}(S_i) = \begin{cases} 0 & \text{if } S_i < S_{i,1} \\ k_{i,\max}\left(\dfrac{S_i - S_{i,1}}{S_{i,2} - S_{i,1}}\right)^{n_i} & \text{if } S_i < S_i < S_{i,2} \quad i = \text{o, w} \\ k_{i,\max} & \text{if } S_{i,2} < S_i \end{cases} \tag{21}$$

$S_{i,1}$ is the lower threshold for a non-zero relative permeability for phase i, while $S_{i,2}$ is the maximal saturation for phase i. Note that these saturations must be given in a consistent way, where $S_{o,1} = 1 - S_{w,2}$ and $S_{w,1} = 1 - S_{o,2}$. The maximal relative phase saturations $k_{i,\max}$ are numbers less or equal to one. The exponents n_i, $i = \text{o, w}$, are usually in the range $1 < n_i < 4$.[38]

The capillary pressure is also given by a power function

$$p_c(S_o) = \begin{cases} p_{c,\min} & \text{if } S_o < S_{o,1} \\ p_{c,\min} + (p_{c,\max} - p_{c,\min})\left(\dfrac{S_o - S_{o,1}}{S_{o,2} - S_{o,1}}\right)^{n_p} & \text{if } S_{o,1} < S_o < S_{o,2} \\ p_{c,\max} & \text{if } S_{o,2} < S_o \end{cases} \tag{22}$$

where $p_{c,\min}$ and $p_{c,\max}$ are the minimal and maximal capillary pressure, respectively. The limiting saturations in the capillary pressure function are the same as those in the oil relative permeability function. The minimal capillary pressure, $p_{c,\min}$, is approximated by zero in the case studies given in later sections.

2.8. Fluid densities and viscosities

The fluid densities of oil and water, ρ_i, $i = \mathrm{o}, \mathrm{w}$, are approximated to first order in pressure p_i and temperature T by

$$\rho_i(p_i, T) = \rho_{i,0}[1 + \alpha_i(p_i - p_{i,0}) - \beta_i(T - T_0)], \quad i = \mathrm{o}, \mathrm{w} \tag{23}$$

where $p_{i,0} = 0$ Pa and $T_0 = 0^\circ\mathrm{C}$ define a reference point where $\rho_i = \rho_{i,0}$. The fluid compressibilities $\alpha_i = (1/\rho_i)(\partial\rho_i/\partial p_i)$ and the thermal expansibilities $\beta_i = -(1/\rho_i)(\partial\rho_i/\partial T)$ are therefore constants of each phase.

Both viscosities, μ_i, $i = \mathrm{o}, \mathrm{w}$, are assumed to be given by explicit functions of the temperature only. The water viscosity will be given by the following function:[39]

$$\mu_\mathrm{w}(T) = \exp\left(\frac{1301}{998{\cdot}333 + 8{\cdot}1855(T-20) + 0{\cdot}00585(T-20)^2} - 1{\cdot}30233\right) \quad 0^\circ\mathrm{C} < T \leqslant 20^\circ\mathrm{C}$$

$$\mu_\mathrm{w}(T) = \mu_{\mathrm{w},0} \exp\left(\frac{1{\cdot}372(20 - T) - 0{\cdot}001053(T-20)^2}{T + 105}\right), \quad 20^\circ\mathrm{C} < T < 200^\circ\mathrm{C} \tag{24}$$

where $\mu_{\mathrm{w},0} = \mu_\mathrm{w}(T = 20^\circ\mathrm{C})$. The oil viscosity is given by the Andrade equation[40]

$$\mu_\mathrm{o}(T) = A \exp\left(\frac{B}{T + 273}\right) \tag{25}$$

where the constants A and B is fitted to a particular oil.

2.9. Specific heat capacities

The specific heat capacities of oil and water c_i, $i = \mathrm{o}, \mathrm{w}$, and the sediments c_s are assumed to be related to temperature by

$$c_i = \frac{\mathrm{d}e_i}{\mathrm{d}T} \quad \text{and} \quad c_\mathrm{s} = \frac{\mathrm{d}e_\mathrm{s}}{\mathrm{d}T}$$

where e_i and e_s are the specific internal energies of fluids and sediments, respectively. The specific heat capacities are assumed constant. No distinction is made between the heat capacities at constant pressure or volume, because the compressibilities and expansibilities of the fluid and the rock matrix are assumed small.

3. THE MODEL

The conservation laws for each fluid phase, the rock matrix and the energy are given in a Lagrangian formulation. These conservation laws are first expressed for a Lagrangian test volume, which will always frame the same ζ-co-ordinates, independent of compaction and kerogen breakdown.

3.1. The conservation of fluid phases

The saturation and pressure equations are derived from oil and water conservation and Darcy's law. Conservation of fluid i in a volume V that follows the compaction in x–y–z-space is

given by

$$\frac{\mathrm{d}}{\mathrm{d}t}\int_V \phi S_i \rho_i \,\mathrm{d}V = -\int_V (\rho_i \mathbf{u}_i)\,\mathrm{d}V + \int_V Q_i \,\mathrm{d}V, \quad i = \mathrm{o}, \mathrm{w} \tag{26}$$

where $\mathbf{u}_i$ is the fluid flux relative to V, and Q_i is a source term. The fluid flux $\mathbf{u}_i$ is given by $\mathbf{u}_i = \phi S_i(\mathbf{v}_i - \mathbf{v}_\mathrm{s})$, where $\mathbf{v}_i$ and $\mathbf{v}_\mathrm{s}$ are the velocities of fluid phase i and the sediment, respectively, in the x–y–z-co-ordinate system. Equation (26) is brought to the x–y–ζ-co-ordinate system, where the $\mathrm{d}/\mathrm{d}t$ operator goes through the integration sign. The integrations are then dropped. (Reference 11.)

$$\frac{\partial}{\partial t}(\phi S_i \rho_i |\mathbf{J}|) + \mathbf{J}^{-1}\nabla'(\rho_i \mathbf{u}_i)|\mathbf{J}| = Q_i |\mathbf{J}|, \quad i = \mathrm{o}, \mathrm{w} \tag{27}$$

The divergence/gradient operators ∇ and ∇' in the x–y–z and x–y–ζ-spaces, respectively, are related by

$$\nabla' = \mathbf{J}\nabla \quad \text{or} \quad \nabla = \mathbf{J}^{-1}\nabla' \tag{28}$$

All quantities in the x–y–ζ-space are marked with a prime to distinguish them form the same quantities in the x–y–z-space. Darcy's law,

$$\mathbf{u}_i = \phi S_i(\mathbf{v}_i - \mathbf{v}_\mathrm{s}) = -\frac{k_{\mathrm{r},i}\mathbf{K}}{\mu_i}(\nabla p_i + \rho_i \mathbf{g}), \quad i = \mathrm{o}, \mathrm{w} \tag{29}$$

relates the fluid flux relative to the sediment particles, to the gradient of fluid pressure and the gravity. The fluid fluxes are proportional to the absolute permeability $\mathbf{K}$ and the phase mobilities $k_{\mathrm{r},i}/\mu_i$.

3.2. *The pressure equation*

The water-excess pressure $p_{\mathrm{w,e}}$, (p for simplicity), and the oil saturation S_o, (S for simplicity), are selected as the main variables. In order to obtain a pressure equation with little explicit dependence on the phase saturations, the conservation laws (27) are first rewritten as

$$|\mathbf{J}|^{-1}\left(\frac{\partial(\phi|\mathbf{J}|)}{\partial t}S_i + \phi|\mathbf{J}|\frac{\partial S_i}{\partial t} + \phi|\mathbf{J}|S_i\frac{1}{\rho_i}\frac{\partial \rho_i}{\partial t}\right) + \frac{1}{\rho_i}\nabla(\rho_i \mathbf{u}_i) = \frac{Q_i}{\rho_i}, \quad i = \mathrm{o}, \mathrm{w} \tag{30}$$

These equations are added to yield

$$\left(\frac{1-\phi}{f}\right)\left(\frac{\partial(ef)}{\partial t} + (ef)\sum_{i=\mathrm{o},\mathrm{w}} S_i \frac{1}{\rho_i}\frac{\partial \rho_i}{\partial t}\right) + \sum_{i=\mathrm{o},\mathrm{w}}\frac{1}{\rho_i}\nabla(\rho_i \mathbf{u}_i) = \sum_{i=\mathrm{o},\mathrm{w}}\frac{Q_i}{\rho_i} \tag{31}$$

where the void ratio is $e = \phi/(1-\phi)$. The time derivative $\partial e/\partial t$ becomes

$$\frac{\partial e}{\partial t} = \frac{\partial e}{\partial \sigma_\mathrm{e}}\frac{\partial \sigma_\mathrm{e}}{\partial t} + \frac{\partial e}{\partial C}\frac{\partial C}{\partial t} \tag{32}$$

since void ratio e is both a function of the effective stress σ_e and the kerogen volume fraction C. The time derivative of the effective stress can be related to the time derivative of the water excess

pressure by use of the definitions constituting (6). The sediment pressure may then be written as a linear relationship with the water excess pressure p and another pressure p_a, which is related to the weight of the material

$$\sigma_\alpha = p_a - p \tag{33}$$

The pressure p_a is

$$p_a = \int_\zeta^{\zeta^*} (\rho_m - \rho_w) g \, d\zeta' - \int_\zeta^{\zeta^*} S_o(\rho_w - \rho_o) g \, d\zeta' - S_o p_c \tag{34}$$

and it may be thought of as a kind of lithostatic pressure. In the absence of hydrocarbons, $S_o = 0$, it is seen that equation (34) becomes the lithostatic pressure

$$p_a = \int_\zeta^{\zeta^*} (\rho_m - \rho_w) g \, d\zeta \tag{35}$$

The time derivatives of the densities are also related to the water-excess pressure

$$\frac{1}{\rho_i}\frac{\partial \rho_i}{\partial t} = \alpha_i \frac{\partial p_i}{\partial t} - \beta_i \frac{\partial T}{\partial t} \tag{36}$$

where the fluid-phase pressures p_i are related to the water excess pressure by

$$p_w = p + p_{w,h} \quad \text{and} \quad p_o = p + p_{w,h} + p_c \tag{37}$$

The fluid fluxes $\mathbf{u}_i$ are expressed by the water-excess pressure p instead of the fluid pressures p_i in the following way:

$$\mathbf{u}_i = \frac{\mathbf{K} k_{r,w}}{\mu_i}(\nabla p_i + \rho_i \mathbf{g}) = \frac{\mathbf{K} k_{r,i}}{\mu_i}(\nabla p + \mathbf{g}_i), \quad i = o, w \tag{38}$$

where

$$\mathbf{g}_w = \mathbf{n}_1 \frac{\partial p_{w,h}}{\partial x} + \mathbf{n}_2 \frac{\partial p_{w,h}}{\partial y} \tag{39}$$

and

$$\mathbf{g}_0 = \mathbf{g}_w + \nabla p_c - (\rho_w - \rho_o)\mathbf{g} \tag{40}$$

When the expressions (32), (36) and (38) are substituted into (31), the pressure equation may be written on the following compact form:

$$C_P \frac{\partial p}{\partial t} - \sum_{i=o,w} \frac{1}{\rho_i} \nabla \left(\frac{\rho_i \mathbf{K} k_{r,i}}{\mu_i}(\nabla p + \mathbf{g}_i) \right) = Q_P \tag{41}$$

where

$$C_P = -\frac{1}{(1-\phi)}\frac{\partial \phi}{\partial \sigma_e} + \phi(S_o \alpha_{o,p} + S_w \alpha_{w,p}) \tag{42}$$

$$Q_P = \frac{Q_o}{\rho_o} + \frac{Q_w}{\rho_w} - \frac{1}{(1-\phi)}\frac{\partial\phi}{\partial\sigma_e}\frac{\partial p_a}{\partial t} - \frac{1}{(1-\phi)}\frac{\partial\phi}{\partial C}\frac{\partial C}{\partial t} - \frac{\phi}{f}\frac{\partial f}{\partial t} + \phi(S_o\beta_o + S_w\beta_w)\frac{\partial T}{\partial t} - \phi\left(S_o\alpha_o\frac{\partial p_{o,h}}{\partial t} + S_w\alpha_w\frac{\partial p_{w,h}}{\partial t}\right) \tag{43}$$

The 'storage' term C_P in the parabolic pressure equation (41) determines how fast pressure transients will decay to a steady-state condition. The 'source' term Q_P is responsible for excess pressure build-up in the basin.

There are other causes of pressure development too. A watertable above sea level will induce meteoric water flow. Furthermore, the gravity terms $\mathbf{g}_i$, $i = o, w$, might be responsible for non-Rayleigh convection or even Rayleigh convection, depending on the thermal gradient, the geometric dimensions and the permeability of a sedimentary layer.[41] Finally, the part $(\rho_w - \rho_o)\mathbf{g}$ in the term $\mathbf{g}_o$ exerts a gravity force on the oil, which will try to redistribute the oil and water towards a gravity stable configuration.

The pressure equation (41) is non-linear in p, because the absolute permeability is non-linear in porosity, which in turn is non-linear in the pressure. This non-linearity is rather weak, which can be seen from a simple estimate of the permeability change

$$\Delta k = -\frac{dk}{d\phi}\frac{\partial\phi}{\partial\sigma_e}\Delta p \tag{44}$$

caused by a change Δp in excess pressure. Recall that $\Delta\sigma_e = -\Delta p$ because of the relation (33). By use of the permeability function (19) and the porosity function (13), the relative change in permeability becomes $\Delta k/k = k_2\phi\alpha\Delta p$. If typical values like $k_2 = 20$, $\phi = 0{\cdot}5$ and $\alpha = 10^{-8}$ Pa^{-1} are used, then an excess pressure change of 1 MPa will lead to a relative change $\Delta k/k = 0{\cdot}1$ (1 MPa is about the weight of 100 m of water).

The boundary conditions which go with the pressure equation (41) are a close boundary, except the basin surface. The basin surface is at zero excess pressure below sea level, or at a given negative hydrostatic pressure along the water table above sea level. The later type of boundary conditions, for the basin surface above the sea level, accounts for meteoric water flow.

3.3. *The saturation equation*

The conservation equation written on the form (30) yields the oil saturation equation

$$C_S\frac{\partial S}{\partial t} - \nabla\left(\rho_o\frac{\mathbf{K}k_{r,o}}{\mu_o}(\nabla p + \mathbf{g}_0)\right) = Q_S \tag{45}$$

where

$$C_S = \phi\rho_o \tag{46}$$

and

$$Q_S = Q_o - \frac{(1-\phi)}{f}S\frac{\partial(ef\rho_o)}{\partial t} \tag{47}$$

This equation together with (41) forms a coupled set of equations for the unknowns p and S.

The saturation equation (45) is solved with zero saturation along the boundaries which are closed for water fluid flow.

3.4. The temperature equation

The temperature equation is derived in a similar manner as the pressure equation. The kinetic energy, the pressure work, the dissipative energy loss and the impact of the gravitational potential are ignored in the energy equation. The derivation starts with conservation of energy in a small test volume V in x–y–z-space that follows the compaction. In such a volume, energy conservation is expressed as

$$\frac{\mathrm{d}}{\mathrm{d}t}\int_V \left(\phi \sum_{i=\mathrm{o,\,w}} \rho_i S_i e_i + (1-\phi)\rho_\mathrm{m} e_\mathrm{s}\right)\mathrm{d}V \tag{48}$$

$$+\int_V \sum_{i=\mathrm{o,\,w}} \nabla(\rho_i e_i \mathbf{u}_i)\,\mathrm{d}V - \int_V \nabla(\lambda \nabla T) = Q_\mathrm{h} \tag{49}$$

where Q_h is an energy source term. Q_h could be the heat production caused by decay of radioactive isotops in the sediments. Then fluid conservation given by (27) is utilized to get

$$C_T \frac{\partial T}{\partial t} + \sum_{i=\mathrm{o,\,w}} \rho_i c_i \mathbf{u}_i \nabla T - \nabla(\lambda \nabla T) = Q_T \tag{50}$$

where the storage term is

$$C_T = \sum_{i=\mathrm{o,\,w}} \rho_i S_i c_i \phi + \rho_\mathrm{m} c_\mathrm{s}(1-\phi) \tag{51}$$

and the general source term is

$$Q_T = Q_\mathrm{h} - \sum_{i=\mathrm{o,\,w}} Q_i e_i - (1-\phi)\rho_\mathrm{m} \frac{1}{f}\frac{\partial f}{\partial t} e_\mathrm{s} \tag{52}$$

The general source term Q_T reduces to the original source term Q_h outside the source rock. However, Q_T is for simplicity set to zero in this paper.

The temperature equation (50) is solved with a given temperature at the basin surface and a given heat flux at the basin bottom.

3.5. Conservation of rock matrix

Anologous to conservation of oil and water in the test volume V, conservation of sediment matrix is expressed as

$$\frac{\mathrm{d}}{\mathrm{d}t}\int_V (1-\phi)\rho_\mathrm{m}\,\mathrm{d}V = \int_V Q_\mathrm{m}\,\mathrm{d}V = -\int_V Q_\mathrm{o}\,\mathrm{d}V = -\int_{V'} Q'_\mathrm{o}\,\mathrm{d}V' \tag{53}$$

where ρ_m is the matrix density. The sink term owing to breakdown of the kerogen part of the matrix is denoted Q_m, and the corresponding oil source term is Q_o. The minus sign is added

because the oil source term corresponds exactly to the mass lost from the solid matrix. The sediment matrix density ρ_m is related to the volume fractions and densities of kerogen and rock in the matrix by

$$\rho_m = \frac{(1 - C_0)\rho_s + \sum_i C_i \rho_{k,i}}{1 - C_0 + C} \tag{54}$$

where $\rho_{k,i}$ and ρ_s are, respectively, the densities of kerogen group i and the rock part of the matrix. These densities are assumed constant. After equation (53) is brought to the x–y–ζ-space, where the derivation operator goes through the integration sign, the source term Q'_o is found to be

$$Q'_o = -\frac{1}{1 - C_0} \sum_i \rho_{k,i} \frac{\partial C_i}{\partial t} \quad \text{or} \quad Q_o = \frac{Q'_o}{|\mathbf{J}|} = -\left(\frac{1 - \phi}{1 - C_0 + C}\right) \sum_i \rho_{k,i} \frac{\partial C_i}{\partial t} \tag{55}$$

This result follows directly from the fact that $C_i/(1 - C_0)$ is the amount of kerogen group i relative to the non-kerogen part of the solid matrix.

3.6. *Comments on the source terms*

So far in the formulation, there are three terms, Q_o, Q_w and Q_m. The water source term, Q_w, is now set to zero, which yields a mass conservative system, because $Q_m = -Q_o$. If a water generating source term is included, for example to model smectite–illite conversion, then the mass of water gained should be accounted for in the solid matrix sink term, in order to preserve mass conservation. With other words, the sum of mass source terms Q_o, Q_w and Q_m should always equal zero.

The terms consitituting the pressure source term Q_P, equation (43), may be arranged into three groups: (1) The term due to compaction, caused by increasing effective stress, which is the term with the factor $\partial\phi/\partial\sigma_e$. (2) The terms owing to the compressibilities and the expansibilities of the fluids, terms with either factor α_i or factor β_i. (3) The terms due to generation of oil from kerogen breakdown.

The impact of kerogen breakdown on the source term Q_P can be studied when the fluids have constant density and the rock matrix does not compact. The only group left in the source term Q_P is then the terms involving kerogen breakdown, and Q_P becomes

$$Q_P = \frac{Q_o}{\rho_o} - \frac{1}{(1 - \phi)} \frac{\partial\phi}{\partial C} \frac{\partial C}{\partial t} - \frac{\phi}{f} \frac{\partial f}{\partial t} \tag{56}$$

It is now possible to obtain simple expressions for Q_P in two situations, one where the porosity is constant, and another, where the porosity is related to the kerogen content by (16).

In the first case, where $\partial\phi/\partial C = 0$, the source term Q_P is

$$Q_P = -\frac{(1 - \phi)}{(1 - C_0 + C)} \sum_i \left(\frac{\rho_{k,i}}{\rho_o} + \frac{\phi_0}{1 - \phi_0}\right) \frac{\partial C_i}{\partial t} \tag{57}$$

In the second case, where $\partial\phi/\partial C = (1 - \phi_0)$, the source term Q_P is

$$Q_P = -\frac{(1 - \phi_0)}{(1 - C_0 + C)} \sum_i \left(\frac{\rho_{k,i}}{\rho_o} - 1\right) \frac{\partial C_i}{\partial t} \tag{58}$$

It is seen from (58) that $\rho_{k,i}/\rho_o > 1$ is a condition for kerogen group i to contribute to pressure build-up, when the space generated by kerogen breakdown adds to the porosity.

It should be noted that the function $f(C)$ is important in the source term Q_P, but not so much in the co-ordinate transformation (1). The z-co-ordinate is not that much dependent on C, because $C \ll 1$ in source rocks, and also because only small parts of a basin are source rocks. However, the various possibilities for dealing with the volume fraction C in the source term Q_P leads to important differences in a source rock, as seen from the two alternatives (57) and (58) for Q_P.

4. NUMERICAL SOLUTION OF THE PRESSURE, SATURATION AND TEMPERATURE EQUATIONS

This section presents the discretization of the pressure equation (41), the saturation equation (45) and the temperature equation (50). The entire basin in x–y–z-space is denoted Ω, while $\partial\Omega$ is the basin boundary. The part of the basin boundary which is open for fluid flow is denoted $\partial\Omega_o$, and the basin bottom is denoted $\partial\Omega_b$.

In the space of basis functions, the excess pressure, the saturation and the temperature are approximated by

$$p = \Sigma_q p_q N_q, \quad S = \Sigma_q S_q N_q \quad \text{and} \quad T = \Sigma_q T_q N_q$$

where N_p is the basis function which is 1 in node p, and zero in all other nodes. Linear line elements are used in 1D, bilinear quadrilateral elements in 2D and linear hexagonal elements in 3D.

4.1. The time discretization

Time discrete equations are made implicit by the backward Euler scheme, which is of order $\mathcal{O}(\Delta t)$. The superscript n is used to denote the time step n, and the step $n+1$ is the current time step. The time derivations carried out in the preceding section are now done by means of the discrete time derivation $\Delta_t f = (f^{n+1} - f^n)/\Delta t$. The time deviation of a product fg is then either

$$\Delta_t(fg) = f^{n+1}\Delta_t g + g^n \Delta_t f \quad \text{or} \quad \Delta_t(fg) = f^n \Delta_t g + g^{n+1}\Delta_t f \tag{59}$$

When the time derivations leading the coefficients C_P, C_S and C_T, and the source terms Q_P, Q_S and Q_T are done by the product rule (59), then the discrete versions of these terms can be written:

$$C_P = -\frac{1}{(1-\phi^{n+1})}\frac{\partial\phi}{\partial\sigma_e} + (1-\phi^{n+1})e^n \frac{f^n}{f^{n+1}} \sum_{i=o,w} S_i^n \alpha_i \tag{60}$$

$$Q_P = \sum_{i=o,w}\frac{Q_i}{\rho_i} - \frac{1}{(1-\phi^{n+1})}\frac{\partial\phi}{\partial\sigma_e}\Delta_t p_a - (1-\phi^{n+1})\frac{e^n}{f^{n+1}}\Delta_t f$$

$$- (1-\phi^{n+1})e^n \frac{f^n}{f^{n+1}} \sum_{i=o,w} S_i^n(\alpha_i \Delta_t p_{i,h} - \beta_i \Delta_t T)$$

$$C_S = \phi^{n+1}\rho_o^{n+1} \tag{61}$$

$$Q_S = Q_o - S^n\left(\phi^{n+1}\rho_o^{n+1} - \frac{f^n}{f^{n+1}}\, e^n(1-\phi^{n+1})\rho_o^n\right)$$

$$C_T = \sum_{i=o,\,w} \rho_i^n S_i^n \phi^n \frac{1-\phi^{n+1}}{1-\phi^n} + (1-\phi^{n+1})\rho_m c_s \tag{62}$$

$$Q_T = Q_h - \sum_{i=o,\,w} Q_i e_i^n - \frac{(1-\phi^{n+1})}{f^{n+1}}\rho_s c_s \Delta_t T$$

It follows from the product rule (59) that there are several possible ways to select which of the factors in these coefficients should be calculated at the time step n or $n+1$. The choice made above has the oil saturation at time n, which makes none of these coefficients directly dependent on S^{n+1}, the main variable S at the current time step.

4.2. The pressure equation

A Galerkin formulation of the pressure equation (41) is made by multiplying the pressure equation by a basis function N_p, and then applying Greens theorem. The discrete pressure equation for node p is then

$$F_p = \int_\Omega \left\{ C_P(p^{n+1}-p^n)N_p + \sum_{i=o,\,w} \Delta t\, \mathbf{K}^{n+1}\left(\frac{k_{r,i}}{\mu_i}\right)_{up,\,i} (\nabla p^{n+1} + \mathbf{g}_i)\rho_i \nabla\left(\frac{1}{\rho_i}N_p\right) \right.$$

$$\left. - \Delta t Q_P N_p \right\} d\Omega = 0 \tag{63}$$

It is well known that a standard Galerkin formulation is unsuited for two-phase flow unless the mobilities $k_{r,i}/\mu_i$ $i = o, w$ are, in some way, evaluated upstream. The mobility for phase i is here evaluated at the node of an element which has the highest excess pressure $p_{e,i}$. The excess pressures $p_{e,i}$ are used to select the upstream direction because they are close to what would have been the fluid flow potentials in case of constant densities. These excess pressures are therefore likely to provide a good estimate for the upstream direction, even in the case of anisotropic absolute permeability. The mobilities can be evaluated either with the saturation at the current time step (implicit) or the previous time step (semi-implicit). The subscript up, i denotes the upstream node for phase i at an element.

Because all boundaries are assumed closed for fluid flow, except the basin surface which is assumed to be at a given excess pressure, the boundary integrals from the Greens formula disappear.

The factors $\rho_i\nabla(N_p/\rho_i)$, $i = o, w$, can be expressed as

$$\rho_i \nabla\left(\frac{N_p}{\rho_i}\right) = \nabla N_p - (\alpha_i \nabla p_i - \beta_i \nabla T_i) N_p \tag{64}$$

which simplifies the numerical evaluation of these factors.

Equation (64) is solved either coupled to the saturation equation or decoupled. When it is decoupled, it is solved with fixed-point iterations (Picard iterations), because the non-linearity in water excess pressure is weak. Notice that equation (64) yields a non-symmetric stiffness matrix, owing to the factors $\rho_i\nabla(N_p/\rho_i)$, $i = o, w$.

4.3. The saturation equation

A Galerkin formulation of the saturation equation is done in the same way as for the pressure equation.

$$G_p = \int_\Omega \left\{ C_S(S^{n+1} - S^n)N_p + \Delta t \rho_o \mathbf{K}^{n+1} \left(\frac{k_{r,o}}{\mu_o} \right)_{up,o} (\nabla p^{n+1} + \mathbf{g}_o) \nabla N_p \right.$$
$$\left. - \Delta t Q_S N_p \right\} d\Omega = 0 \tag{65}$$

The mobility $k_{r,o}/\mu_o$ is evaluated at the upstream node of an element, pointed out by the oil excess pressure $p_{e,o}$, as done for the same term in the pressure equation.

No boundary integrals remain from the Greens formula, because all boundaries, except those at hydrostatic pressure, are assumed to be closed to fluid flow.

4.4. The temperature equation

The temperature equation is obtained by standard Galerkin formulation

$$H_p \int_\Omega \left\{ C_T(T^{n+1} - T)N_p + \sum_{i=o,w} \Delta t \rho_i c_i \mathbf{u}_i^n \nabla T^n N_p \right.$$
$$\left. + \Delta t \lambda \nabla T^{n+1} \nabla N_p - \Delta t Q_T N_p \right\} d\Omega + \Delta t \int_{\partial\Omega_b} \mathbf{q}_b \mathbf{n} N_p \, ds = 0 \tag{66}$$

The temperature equation (66) is linear since there is no temperature dependence in the thermal conductivity λ or the coefficient C_T. Note that the stiffness matrix obtained from (66) is symmetric since the advective term is explicit in time.

4.5. Computation of coupled pressure, saturation, temperature and compaction

The pressure, the saturation, the temperature and the compaction are coupled, and these quantities are solved for in a loop which runs until 'convergence' in pressure and saturation. This iterative loop is slightly different depending on whether pressure and saturation are solved coupled or decoupled. These four steps constitute the loop when pressure and saturation are decoupled: (1) solve for pressure, (2) use the pressure solution to update the porosity, and also the x–y–z-grid (3) solve for temperature, and (4) solve for saturation. Step four falls out when pressure and saturation are coupled, in which case both are solved for in step (1). The x–y–z-grid is obtained from the x–y–ζ-grid in step (2) by the transformation (1). In case of only water, $S_o = 0$, the pressure equation (41) is seen to reduce to the pressure equation for one-plane flow and compaction. A FEM for this special case is studied in an earlier paper.[11]

The Jacobian in case of a coupled pressure and saturation equation is given in the appendix.

5. GLOBAL MASS BALANCE

The global mass balance of oil in the basin at time t^n is

$$\int_{\Omega^n} \phi \rho_o S \, dV = \int_{t_0}^{t_n} \int_{\Omega(t)} Q_o \, dx \, dt - \int_{t_0}^{t_n} \int_{\partial\Omega_o(t)} \mathbf{u}_o \mathbf{n} \, dA \, dt \tag{67}$$

The mass of oil in the pore volume of the basin is equal to the total amount of oil generated, minus the total amount of oil lost through the open boundaries of the basin. The open boundaries are denoted $\partial\Omega_o(t)$ at time t. The amount of oil generated is easily calculated by subtracting the mass of kerogen the basin would have had if there had been no oil generation, from the actual mass of kerogen left in the basin, which is

$$M^n = \int_{\Omega^n} \frac{(1-\phi)}{(1-C_0+C)} \sum_i \rho_{k_i} C_i \, \mathrm{d}x \tag{68}$$

The total mass of kerogen in the basin in case of oil generation, M_0^n, is given by equation (68) when $C = C_0$. As long as no oil leaks out of the basin (the computational domain), the mass of oil in the porous volume of the basin is simply

$$\int_{\Omega^n} \phi \rho_o S \, \mathrm{d}V = M_0^n - M^n \tag{69}$$

It is therefore easy to check the mass balance, especially since there is no flow out of the boundaries.

6. VALIDATION OF THE MODEL

6.1. A 1D fractional flow-based migration model

The model is validated by comparisons with results from a 1D migration model based on a fractional flow formulation of the conservation laws for oil and water.[38] The fractional flow formulation in 1D allows for solving the saturation equation without explicitly solving the pressure equation. Such a formulation also offers process insight, when made dimensionless by proper scaling. The following dimensionless saturation equation can be derived from conservation of each phase in the vertical direction, using equations (27),

$$\frac{\partial}{\partial\tau}\left(e_0\left(1+\frac{C}{1-C_0}\right)S\right) - \frac{\hat{\zeta}}{\tau}\frac{\partial}{\partial\hat{\zeta}}\left(e_0\left(1+\frac{C}{1-C_0}\right)S\right) + \frac{1}{\tau}\frac{\partial F}{\partial\hat{\zeta}} = -\frac{1}{1-C_0}\left(\frac{\partial C}{\partial\tau}\right)_\zeta \frac{\rho_k}{\rho_o} \tag{70}$$

See Reference 28, where this equation is derived. The scaling leading to the dimensionless formulation (70) is

$$\begin{aligned} \hat{\zeta} &= \zeta/(\omega t) \\ \tau &= t/t_0 \\ \hat{u}_t &= u_T/\omega \\ \hat{p}_c &= p_c/p_0 \end{aligned} \tag{71}$$

where quantities with a hat above are dimensionless. The burial rate measured as porosity free rock is ω, which is a characteristic velocity of the problem. Only one kerogen group is used for simplicity, and the half-life of the selected kerogen group is used as the characteristic time t_0. Time is not measured by pore volumes, since there is no characteristic pore volume of the model, owing to the basin growing in time. Pressure is scaled by the characteristic buoyancy pressure at the time t_0, which is $p_0 = (\rho_w - \rho_0) g\omega t_0$. The phase densities are assumed different, in order to have $p_0 \neq 0$. Furthermore, it is assumed a constant void ratio e_0, and that capillary pressure gradients are negligible, which is a reasonable assumption for a homogeneous rock and long length scales.

The ζ-subscript on the time derivation on the right-hand side tells that the ζ-co-ordinate, (not the $\hat{\zeta}$-co-ordinate), is kept constant under the derivation.

The fractional flow function is

$$F = f_o(S)\hat{u}_T(\hat{\zeta}, \tau) + N_G f_o(S) k_{rw}(1 - S) \tag{72}$$

where the gravity number

$$N_G = \frac{k_o(\rho_w - \rho_o)g}{\mu_w \omega} \tag{73}$$

is an important parameter in this simple model. The mobilities of the fluid phases are denoted $\lambda_i = k_{r,i}/\mu_i$, $i = o, w$, and the fraction flow functions for each phase are $f_i = \lambda_i/(\lambda_o + \lambda_w)$, $i = o, w$. The viscosities μ_i, $i = o, w$ are assumed constant, which implies that the mobilities and the fractional flow functions become functions of the saturation only. It should be noted that the ratio of the viscosities appear as a parameter in the functions f_i, $i = o, w$. The total volumetric velocity $\hat{u}_T = u_T/\omega$, where $u_T = u_{o,z} + u_{w,z}$, is given by

$$\hat{u}_T(\hat{\zeta}, \tau) = \tau \frac{1}{(1 - C_0)} \left(\frac{\rho_k}{\rho_o} + e_0 \right) \int_0^{\hat{\zeta}} \left(\frac{\partial C}{\partial \tau} \right)_\zeta d\hat{\zeta}' \tag{74}$$

The gravity number will differentiate between two different regimes, one where gravity is important, $N_G \gg 1$, and another where gravity is less important, $N_G \ll 1$. In the last regime, of negligible gravity, the driving force for the oil is simply the source term for oil, which forces both oil and water out of the pore space. It is seen from (73) that low permeability and high deposition rate reduce the importance of gravity, while the opposite, high permeability and low deposition rate increase the importance of gravity.

6.2. Two 1D test examples

Solutions of the dimensionless saturation equation (70), when the total velocity $\hat{u}_T$ is given by (74), are used as reference solutions for the full model. The reference solution is obtained by an upstream finite difference schemes as described in Reference 28. This model is denoted the 'reference model' to distinguish it from the FEM-based full model.

Two cases are selected, a gravity dominated case with $N_G = 10$, and a case where gravity is less important, $N_G = 0{\cdot}5$. Additional input data common for both the reference model and the full model are given in Tables I and Table II. Both models have the same thermal history, which is given by a constant thermal gradient, $\partial T/\partial z = 0{\cdot}04°C/m$.

The two different versions of the full model are subsequently denoted FEM1, and FEM2, where the FEM1 is the FE-based saturation equation solved decoupled from the pressure, while FEM2 is coupled.

The FEM2 saturation solution is in Figure 1 as a solid thin line, where it is compared with the reference solution (thick line). The solutions are shown in Figure 1 at several time steps, until the saturation front reaches the basin top. The half-life of the kerogen group given in Table I is $t_0 = 20{\cdot}7$ Ma for the linear increase in temperature in this case. The time span of the case is 60 Ma, which means that the dimensionless time span is $\tau_{max} = 2{\cdot}9$. The saturation solutions are plotted at eight different times: from $\tau = 1{\cdot}2$ ($t = -35{\cdot}2$ Ma) to $\tau = 2{\cdot}4$ ($t = -6{\cdot}3$ Ma) by a time step $\Delta\tau = 0{\cdot}2$ ($\Delta t = 4{\cdot}13$ Ma). It is seen from Figure 1 that not enough oil is generated for oil to flow until about $\tau = 1{\cdot}4$ ($t = -31{\cdot}0$ Ma). This is consistent with the half-life, $\tau = 1$, of the kerogen group. Notice that the residual oil saturation is 0·2, which means there is no flow unless the saturation is larger than this threshold.

Table I. Common input data

A (Arrhenius factor)	$1{\cdot}0 \times 10^{12}$ (1/s)
E (activation energy)	200·0 (kJ/mol)
ω (burial rate)	100·0 (m/Myr)
ρ_k/ρ_o (volume expansion)	1·5 (dimensionless)
$S_{i,1}$ (lower threshold for saturation)	0·2 (dimensionless)
$S_{i,2}$ (upper threshold for saturation)	0·2 (dimensionless)
n_o (relative permeability exponent)	3 (dimensionless)
n_w (relative permeability exponent)	3 (dimensionless)
ϕ_0 (porosity)	0·1 (dimensionless)
C_0 (initial kerogen concentration)	0·05 (dimensionless)

Table II. Full model input data

μ_o (oil viscosity)	0·002 (Pa s)
μ_w (water viscosity)	0·001 (Pa s)
ρ_k (kerogen density)	1150 (kg/m^3)
ρ_o (oil density)	750 (kg/m^3)
ρ_w (water density)	1000 (kg/m^3)
k (absolute permeability, $N_G = 10$)	$1{\cdot}3 \times 10^{-17}$ (m^2)
k (absolute permeability, $N_G = 0{\cdot}5$)	$6{\cdot}5 \times 10^{-19}$ (m^2)

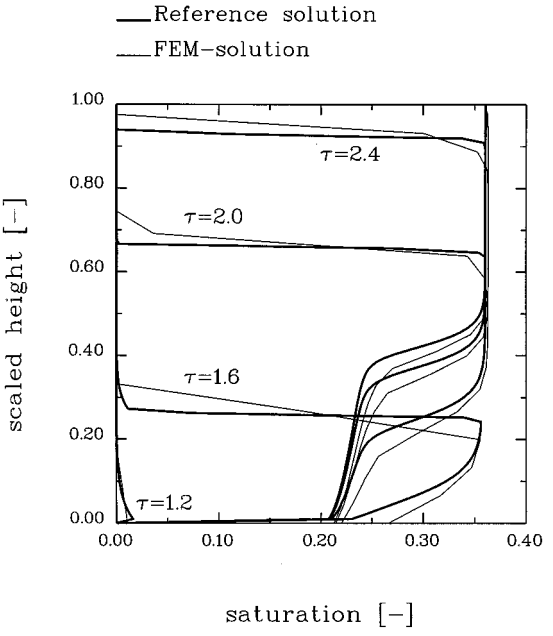

Figure 1. A plot of the 1D reference solution (thick line) compared with the FEM2 solution (thin solid line) for the case $N_G = 10$ at four different times: from $\tau = 1{\cdot}2$ ($t = -35{\cdot}2$ Myr) to $\tau = 2{\cdot}4$ ($t = -6{\cdot}3$ Myr) by a time step $\Delta\tau = 0{\cdot}4$ ($\Delta t = 8{\cdot}26$ Myr). These solutions are seen to be in good agreement. The saturation solution is easily identified as a shock moving upwards, which finally reaches the surface

As seen from Figure 1, the FEM2 solution is in good agreement with the reference solution. The mass balance error for this case, ($N_G = 10$), is shown until breakthrough in Figure 2. The error is calculated with the expression (69), and the right-hand side, $M_0^n - M^n$ is shown with the thick line and the left-hand side $\int_{\Omega^n} \phi \rho_0 S \, dV$ is shown with the thin line. The right-hand side, which is the weight of kerogen converted to oil, and the left-hand side which is the weight of oil in the basin, follow each other closely. They differ by much less than 1 per cent.

The gravity is the dominant force in this case, which is also seen from the saturation solution in Figure 1. The solution is basically a shock moving faster relative to the sediment grains than the source region where most of the kerogen breakdown takes place (see Reference 28 for more details).

The gravity is less important in the next case of $N_G = 0{\cdot}5$. The saturation solution of FEM2, together with the reference solution of this case, is shown in Figure 3. The plot shows the solutions at several time steps, but there is no breakthrough. The saturation can be shown to follow the source region as it moves away from the basin bottom.[28]

The mass balance for FEM2, shown in Figure 4, is seen to be less than 1 per cent, just as in the case $N_G = 10$. Figures 3 and 4 show, just as for the previous case, that the FEM2 solution is in good agreement with the reference solution.

7. A 2D CASE EXAMPLE

7.1. *Case description*

The model is applied to a simple 2D example case to demonstrate the modelling of oil expulsion from the source rock, the secondary migration of oil in a carrier bed and the trapping of oil.

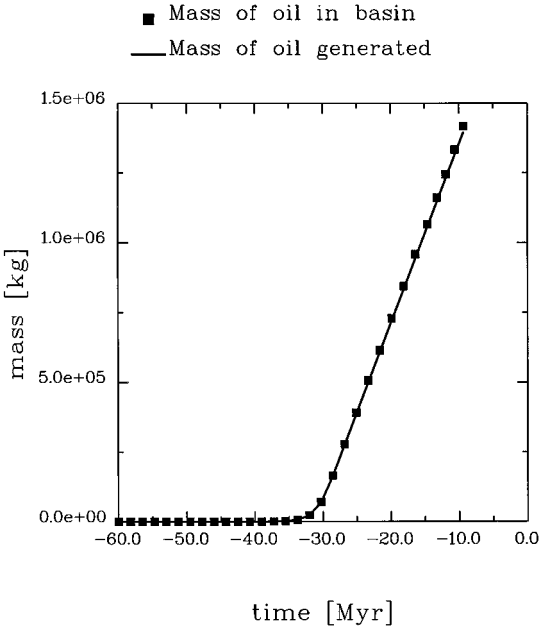

Figure 2. The plot shows the mass balance error of FEM2 for the case $N_G = 10$ by comparing the mass of kerogen converted to oil with the mass of oil in the basin

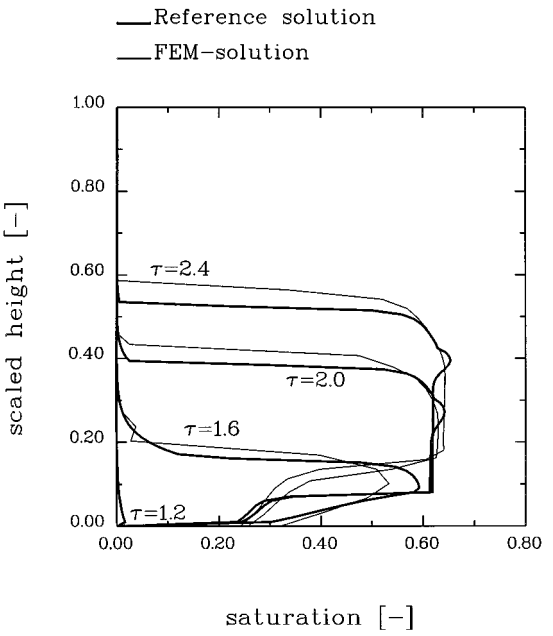

Figure 3. A plot fo the 1D reference solution (thick line) compared with the FEM2 solution (thin line) for the case $N_G = 10$ at 4 different times: from $\tau = 1{\cdot}2$ ($t = -35{\cdot}2$ Myr) to $\tau = 2{\cdot}4$ ($t = -6{\cdot}3$ Myr) by a time step $\Delta\tau = 0{\cdot}4$ ($\Delta t = 8{\cdot}26$ Myr). These solutions are seen to be in good agreement. The saturation does not reach the surface in this case

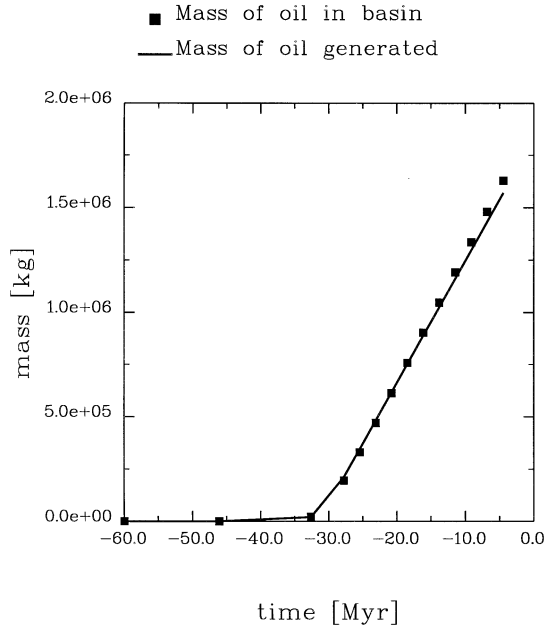

Figure 4. The plot shows the mass balance error of FEM2 for the case $N_G = 0{\cdot}5$ by comparing the mass of kerogen converted to oil with the mass of oil in the basin

The case consists of the deposition of 4 lithologies, which are shown in Figure 5, where the time spans of their deposition are shown too. The basin begins with the deposition of ShaleBot at the centre part of the basin and SourceRock deposited at the sides. See Tables III and V for the

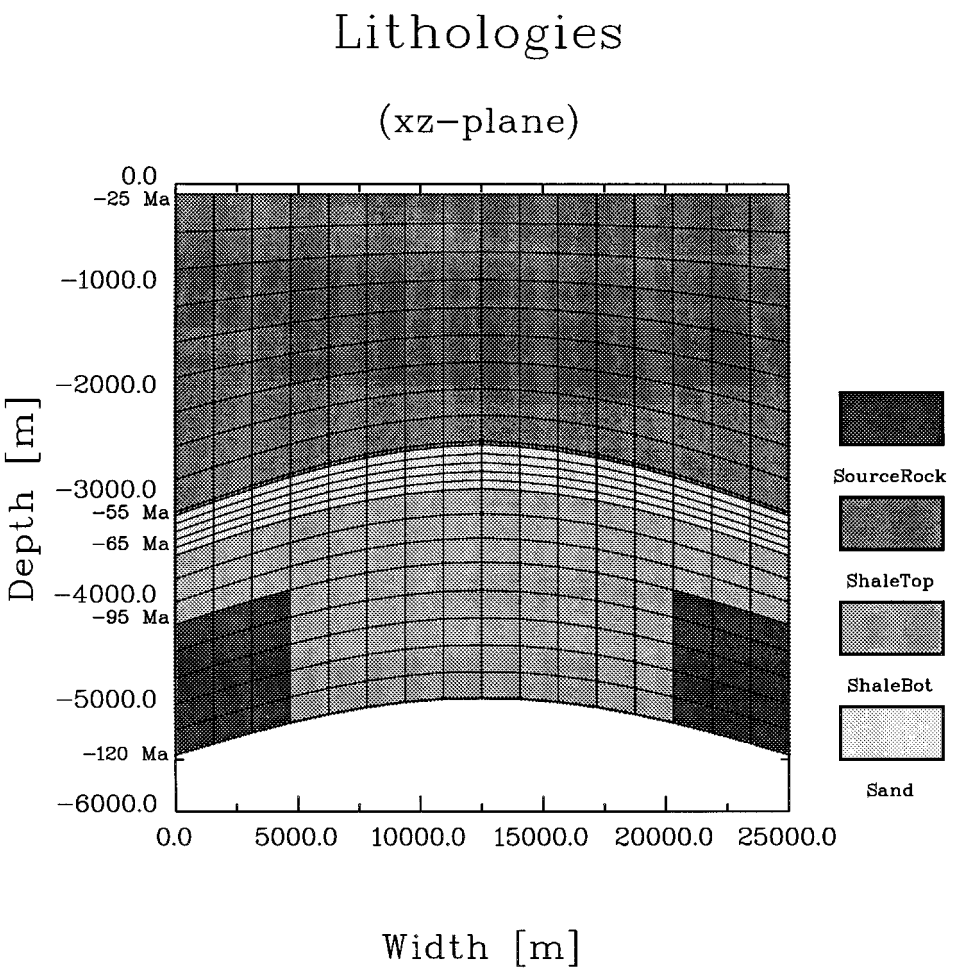

Figure 5. The lithologies comprising the basin. The SourceRock is deposited from −120 to −95 Myr at the flanks of the basin with ShaleBot in the centre. These lithologies have the same properties except that SourceRock has a hydrocarbon potential, and they are deposited with the same sedimentation rates. Then follows a ShaleBot formation from −95 to −65, a Sand layer from −65 to −55 Myr and finally the Shale from −55 to −25 Myr. There is no deposition from −25 Myr until present

Table III. Parameters common for the lithologies of the 2D case

Parameter	Value	Units
ρ_s	2600	$(kg\,m^{-3})$
c_s	1000·0	$(kg^{-1}\,K^{-1})$
λ_s	4·0	$(W\,m^{-1}\,K^{-1})$
α	$1{\cdot}0\times10^{-8}$	(Pa^{-1})

parameters defining the lithologies. ShaleBot and SourceRock have the same properties, except that the SourceRock is rich is kerogen, while ShaleBot does not contain any kerogen. The kerogen content and the kinetic parameters of the kerogen groups in the SourceRock are given by Table VI. Then follows the ShaleBot lithology from -95 to -65 Ma, the Sand lithology from -65 to -55 Ma, the Shale lithology from -55 to -25 Ma and finally there is 'pause' until present. All layers have the same thickness until the last shale (ShaleTop), which forms the symmetrically shaped dome by being thicker at the sides than at the centre. The fluid properties of both the oil and water are given in Table VII.

The saturation and the oil Darcy velocities are plotted at 4 times during the simulation of the basin, at -50, -25, -10 Ma and at present, see Figures 6–9. At time -50 Ma, which is at the beginning of the deposition of the last lithology, ShaleTop, Figure 6 shows that the oil starts to leave the source rock. The Darcy velocities in Figure 6 show that the expulsion of oil from the source rock is a slow process in this case, with Darcy velocities around 5 m/Ma. At the end of the deposition of ShaleTop, at -25 Ma, the oil fills the carrier bed, as seen from Figure 7. The Darcy velocities in the carrier bed are larger than in the source rock, or order 10 m/Ma. The trap starts to fill at the time -10 Ma, as seen from Figure 8. Finally, the saturation at present is given in Figure 9. The trap is still being filled, but at a lower rate, with a oil–water contact about in the middle of the sand layer.

Table IV. Permeability and porosity data for the lithologies of the 2D case

Name	k_1 (m^2)	k_2	K_1/K_3	ϕ_0
Sand	$1{\cdot}0\times10^{-15}$	0	500	0·5
ShaleBot	$1{\cdot}0\times10^{-21}$	20	1	0·4
ShaleTop	$1{\cdot}0\times10^{-23}$	20	1	0·4
SourceRock	$1{\cdot}0\times10^{-21}$	20	1	0·4

Table V. Relative permeability and capillary pressure data for the lithologies of the 2D case

Name	$S_{i,1}$	$S_{i,2}$	n_i	$k_{i,\max}$	n_p	$p_{c,\max}$ (Pa)
Sand	0·05	0·95	2	1	2	$5{\cdot}0\times10^{3}$
ShaleBot	0·1	0·9	2	1	2	$1{\cdot}0\times10^{5}$
ShaleTop	0·1	0·9	2	1	2	$1{\cdot}0\times10^{7}$
SourceRock	0·1	0·9	2	1	2	$1{\cdot}0\times10^{5}$

Table VI. The kerogen content of the source rock

E_i (kJ mol^{-1})	A_i (s^{-1})	$C_{0,i}$	$\rho_{k,i}$ (kg m^{-3})
150	$1{\cdot}0\times10^{+17}$	0·01	1500
160	$1{\cdot}0\times10^{+17}$	0·01	1500
170	$1{\cdot}0\times10^{+17}$	0·01	1500
180	$1{\cdot}0\times10^{+17}$	0·01	1500
190	$1{\cdot}0\times10^{+17}$	0·01	1500

Table VII. The fluid data in the 2D case

		Fluid data	
Property	Units	Oil ($i = o$)	Water ($i = w$)
ρ_i	($kg\,m^{-3}$)	700·0	1000·0
α_i	(Pa^{-1})	$2{\cdot}0 \times 10^{-9}$	$5{\cdot}0 \times 10^{-10}$
β_i	(K^{-1})	$8{\cdot}0 \times 10^{-4}$	$2{\cdot}0 \times 10^{-4}$
c_i	($J\,kg^{-1}\,K^{-1}$)	4500·0	4180·0
λ_i	($W\,m^{-1}\,K^{-1}$)	0·5	0·63
A	(Pa s)	$2{\cdot}75 \times 10^{-6}$	(Only oil)
B	(K)	2198·5	(Only oil)

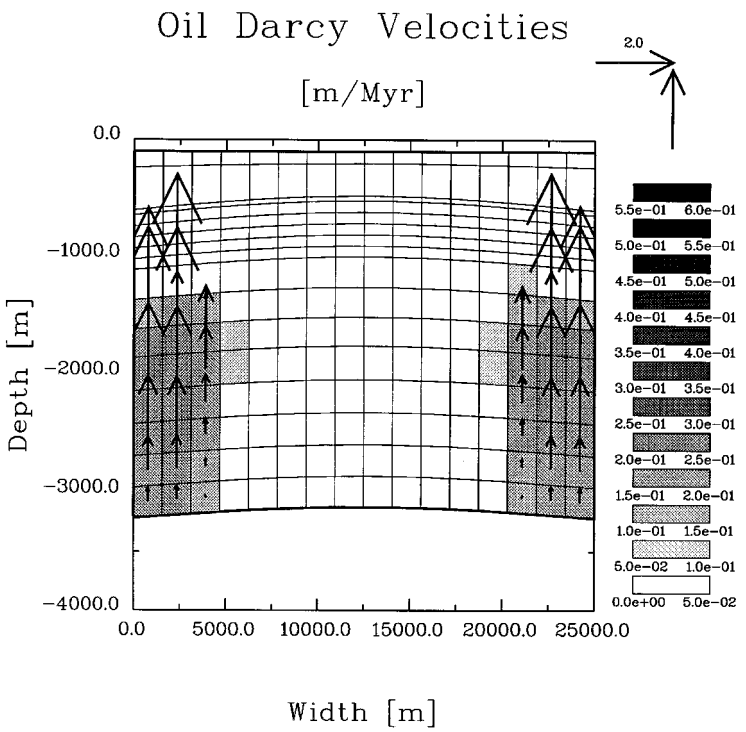

Figure 6. The oil saturation and the oil Darcy velocities at time = − 50 Myr

The FEM2 formulation was used in this 2D case, and the saturation solution is seen to be symmetric at the four different stages shown. The mass balance error is shown in Figure 10, by comparing the left and the right sides of expression (69), and it seen to be less than 5 per cent throughout the simulation. This error is considered acceptable compared with the uncertainties associated with the geological data, as for instance the amount of kerogen in the source rocks. The five small bumps on the curves of mass of oil in system in Figure 10 are due to the low

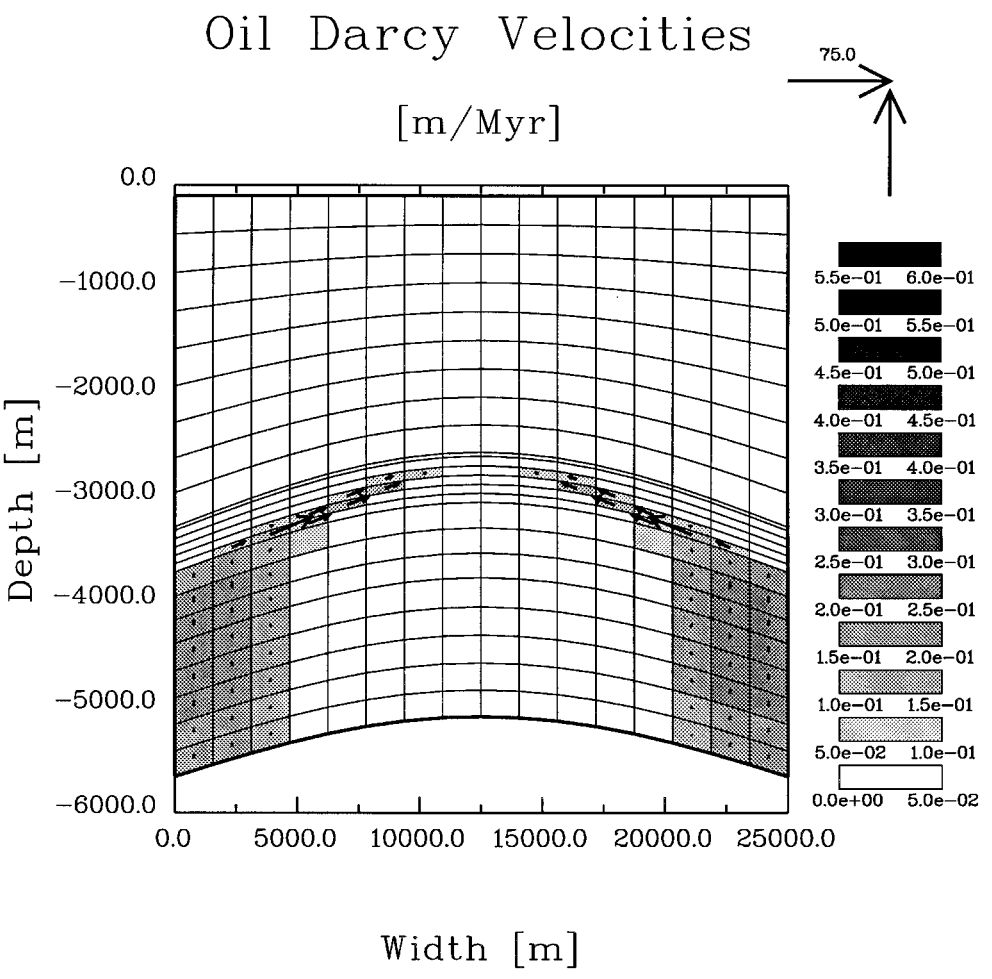

Figure 7. The oil saturation and the oil Darcy velocities at time = − 25 Myr

resolution of the source rock, only five cells in the vertical direction. This plot also shows that no more oil is generated after − 55 Ma, when the kerogen potential is exhausted.

7.2. Some comments to the case

It is important to notice the Sand lithology has an anisotropic permeability, being 500 times more permeable in the lateral direction than in the vertical direction. This anisotropy was introduced in order to have sufficient lateral flow to fill the trap. A moderately permeable and isotropic sandstone would imply little lateral flow. An isotropic sandstone with a large permeability might provide sufficient lateral flow in the carrier bed to fill the trap. However, buoyancy driven migration in carrier beds with a large permeability, for instance permeabilities above 1D, is challenging to model on a geological time scale. This is easily seen from a simple estimate of the

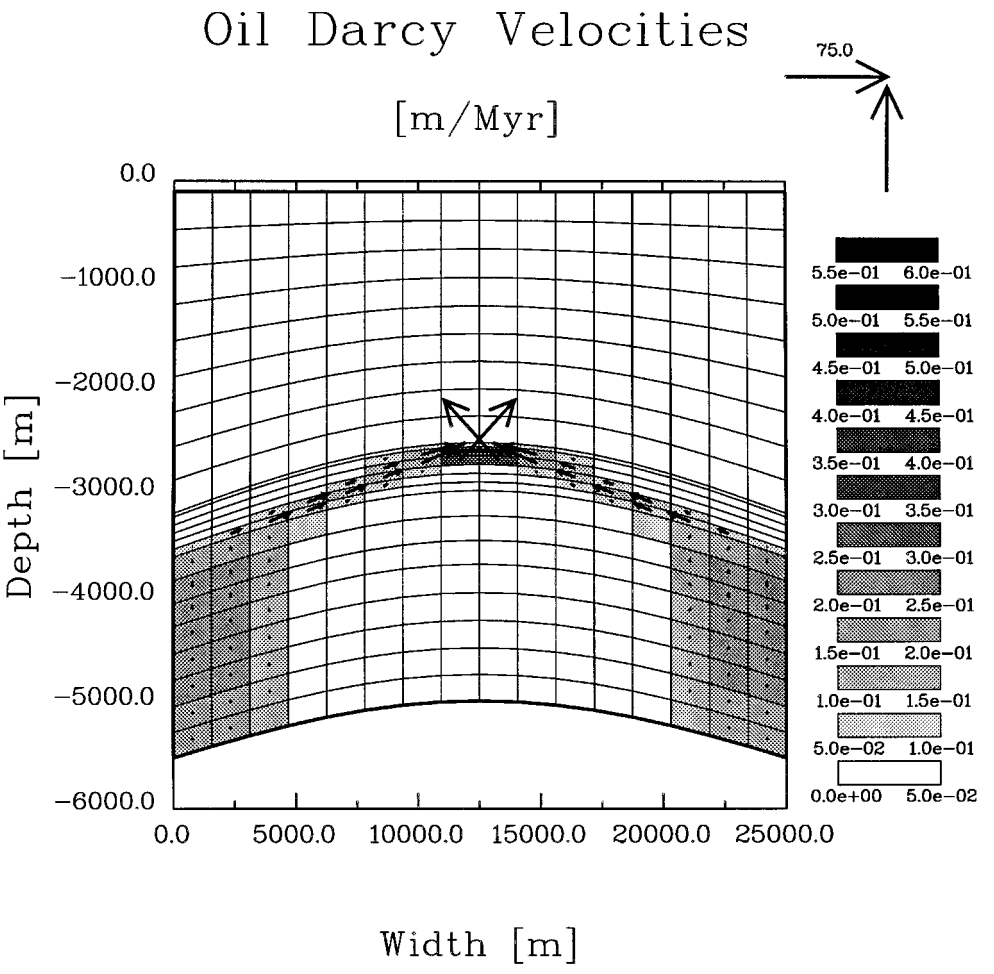

Figure 8. The oil saturation and the oil Darcy velocities at time = − 10 Myr

oil Darcy velocity along a carrier bed owing to buoyancy

$$u_o = \frac{k\, k_{r,o}}{\mu_o}(\rho_w - \rho_o) g \sin\theta \tag{75}$$

where θ is the angle of inclination. With $k = 1\text{D}$ and the values from Table VIII, the lateral velocity in the carrier bed is $u_o = 3{\cdot}15 \times 10^5$ m/Ma. Even with a 1000 m wide finite elements, this will require small time steps, possibly of order 0·001 Ma, depending on the porosity. Furthermore, a carrier bed with an absolute permeability in the range from 100 mD and upwards is likely to become gravity segregated when it is slowly charged with oil. Gravity segregation takes place when the capillary/gravity transition zone is much less than the carrier bed thickness. A fluid flow type, like gravity segregated flow, is difficult to model.

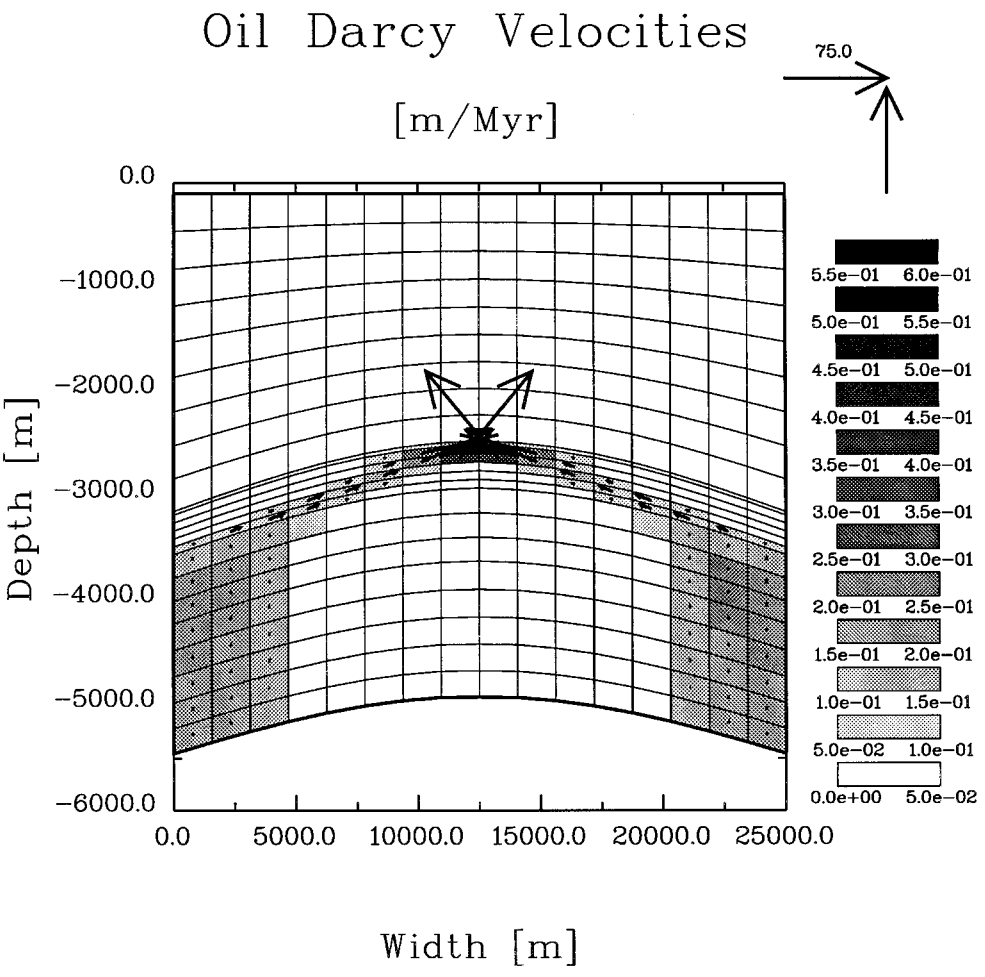

Figure 9. The oil saturation and the oil Darcy velocities at present

Finally, it should be noted that the FEM-saturation solution is a continuous field given at the nodes of the grid. The saturation values shown in the Figures 6–9 are average values for each element. This piecewise constant way of representing the FEM-solution implies that the shale-elements above the trap in Figure 9 have small saturations. This shale layer is therefore discretized by a thin row of elements above the carrier bed to restrict this effect.

8. CONCLUSION

A FEM-model of immiscible two-phase oil migration is formulated for compacting sedimentary basins, where the compaction takes place in the vertical direction. The model is based on a Lagrange formulation where the Lagrangian co-ordinate is the height of the completely compacted rock without any oil potential. The pressure equation, derived in the Lagrangian

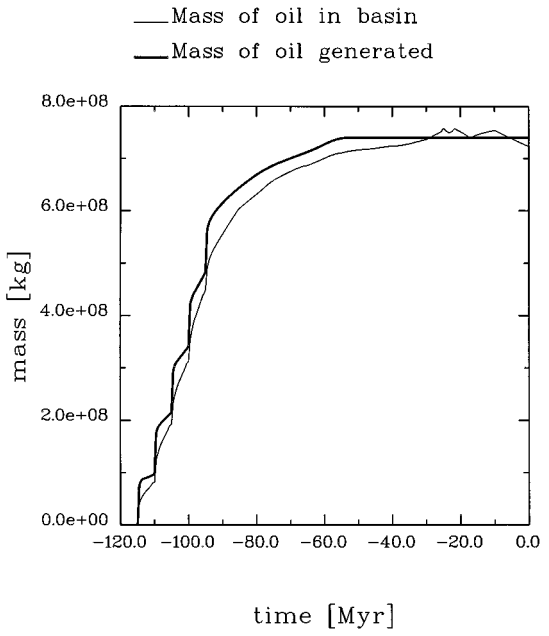

Figure 10. The plot shows the mass balance error of FEM2 for the 2D case example by comparing the total mass of kerogen converted to oil with the total mass of oil in the basin. These two quantities differ by less than 5 per cent

Table VIII. Parameters used to calculate a lateral oil Darcy velocity

Parameter	Value	Units
k	$1{\cdot}0 \times 10^{-12}$	(m^2)
$k_{r,o}$	0·1	
μ_o	$2{\cdot}5 \times 10^{-3}$	(Pa s)
$(\rho_w - \rho_o)g$	2500	(Pa/m)
$\sin\theta$	0·01	

co-ordinates, accounts directly for these causes of pressure generation in the basin: (1) compaction (2) fluid density variations and (3) generation of oil from kerogen. The eventual pore-space generated by breakdown of kerogen is considered. The thermal density variations, which may be responsible for convection, appear in a direct manner in the formulation.

The simple and straightforward upstream-weighted FEM with mass-lumping is applied to the modelling of immiscible two-phase oil migration. This approach is validated by comparison with a 1D dimensionless migration model, based on the fractional flow formulation. The FEM-based model compares well with the 1D reference model, where the saturation equation is solved with a standard finite-difference scheme, with upstream mobilities. The applicability of the model to a 2D test case, including both primary and secondary migration, and the filling of an anticlinal, is demonstrated. The mass balance of the test cases was checked because the finite element formulation does not enforce exact mass conservation. The 1D test cases showed excellent mass blance, while the 2D case had less than 5 per cent mass balance error.

The upstream-weighted FEM with mass-lumping is a good first alternative for modelling oil migration. This conclusion relies on the experience with the method, together with the fact that this FEM is as easily implemented as any standard FEM.

ACKNOWLEDGEMENTS

This work has been funded by grants from the Norwegian Research Council (NFR) and Institutt for Energiteknikk. The author is grateful to his colleague Egil Brendsdal for discussion concerning hydrocarbons, and to the comments and suggestions provided by the reviewers, as well as the editorial handling by C.S. Desai.

APPENDIX

The Jacobian of the coupled pressure and saturation equations

The Jacobian of the coupled pressure and saturation equation is a block-matrix, where each block is given by

$$\begin{pmatrix} \dfrac{\partial F_p}{\partial p_q} & \dfrac{\partial F_p}{\partial S_q} \\ \dfrac{\partial G_p}{\partial p_q} & \dfrac{\partial G_p}{\partial S_q} \end{pmatrix} \tag{76}$$

These matrix elements are given below:

$$\frac{\partial F_p}{\partial p_q} = \int_\Omega \left\{ G_P N_p N_q + \sum_{i=\mathrm{o,w}} \Delta t p \mathbf{K}^{n+1} \left(\frac{k_{\mathrm{r},i}}{\mu_i} \right)_{\mathrm{up},i} \nabla N_q \rho_i \nabla \left(\frac{1}{\rho_i} N_p \right) \right\} \mathrm{d}\Omega \tag{77}$$

$$\frac{\partial F_p}{\partial S_q} = \int_\Omega \left\{ \sum_{i=\mathrm{o,w}} \Delta t \mathbf{K}^{n+1} \left(\frac{1}{\mu_i} \frac{\mathrm{d}k_{\mathrm{r},i}}{\mathrm{d}S} \right)_{\mathrm{up},i} \delta_{(\mathrm{up},i),q} (\nabla p^{n+1} + \mathbf{g}_i) \rho_i \nabla \left(\frac{1}{\rho_i} N_p \right) \right\} \mathrm{d}\Omega \tag{78}$$

$$\frac{\partial G_p}{\partial p_q} = \int_\Omega \left\{ \Delta t \rho_\mathrm{o} p \mathbf{K}^{n+1} \left(\frac{k_{\mathrm{r,o}}}{\mu_\mathrm{o}} \right)_{\mathrm{up,o}} \nabla N_p \nabla N_q \right\} \mathrm{d}\Omega \tag{79}$$

$$\frac{\partial G_p}{\partial S_q} = \int_\Omega \left\{ C_S \delta_{p,q} + \Delta t \rho_\mathrm{o} \mathbf{K}^{n+1} \left(\frac{1}{\mu_\mathrm{o}} \frac{\mathrm{d}k_{\mathrm{r,o}}}{\mathrm{d}S} \right)_{\mathrm{up,o}} \delta_{(\mathrm{up,o}),q} (\nabla p^{n+1} + \mathbf{g}_\mathrm{o}) \right\} \mathrm{d}\Omega \tag{80}$$

Notice that the derivation is only done with respect to explicit pressure dependence. In an earlier paper,[11] the derivation was also done with respect to porosity and the porosity-dependent permeability. Experience shows that this simple scheme is sufficient, due to the weak non-linearities caused in porosity and permeability. The size of the non-linearity in permeability is estimated by (44) and in the paragraph below.

The Kronecker delta $\delta_{p,q}$ is zero, except when $p = q$, when it is 1. The node (up, i) denotes the upstream node for phase i on an element.

REFERENCES

1. P. A. Allen and J. R. Allen, *Basin Analysis: Principles and Applications*, Blackwell Scientific Publications, Oxford, 1990.
2. D. M. Audet and A. C. Fowler, 'A mathematical model for compaction in sedimentary basins', *Geophys. J. Int.*, **110,** 577–590 (1992).

3. C. M. Bethke, 'A numerical model of compaction-driven groundwater flow and heat transfer and its application to the paleohydrology of intracratonic sedimentary basins', *J. Geophys. Res.*, **90,** 6817–6828 (1985).
4. C. M. Bethke and T. F. Corbet, 'Linear and nonlinear solutions for one-dimensional compaction flow in sedimentary basis', *Water Resour. Res.*, **24,** 461–467 (1988).
5. J. D. Bredehoeft and B. B. Hanshaw, 'On the maintenance of anomalous fluid pressures, I., thick sedimentary sequences', *Geol. Soc. Amer. Bull.*, **79,** 1097–1106 (1968).
6. R. E. Gibson, 'The progress in consolidation in a clay layer increasing in thickness with time, *Geotechniquee*', **8,** 171–182 (1958).
7. Y. Shi and C.-Y. Wang, 'Pore pressure generation in sedimentary basins: overloading versus aquathermal', *J. Geophys. Res.*, **91,** 2153–2162 (1986).
8. J. E. Smith, 'The dynamics of shale compaction and evolution in pore-fluid pressures', *Math. Geol.*, **3,** 239–262 (1971).
9. J. Søreng, 'Formulation and application of element methods in the numerical simulation of geological basins', *Int. j. numer. anal. methods geomech.*, **13,** 525–543 (1989).
10. M. Wangen, 'Pressure and temperature evolution in sedimentary basins', *Geophys. J. Int.*, **110,** 601–613 (1992).
11. M. Wangen, 'A finite element formulation in Lagrangian coordinates for heat and fluid flow in compacting sedimentary basins', *Int. j. numer. anal. methods geomech.*, **17,** 401–432 (1993).
12. C. Hermanrud, 'Basin modelling techniques—an overview', in A. G. Doré *et al.* (eds), *Basin Modelling: Advances and Applications* NPF Special Publication 3, Elsevier, Amsterdam, 1993, pp. 1–34.
13. P. Ungerer, J. Burrus, B. Doligez, P. Y. Chenet and F. Bessis, 'Basin evaluation by integrated two-dimensional modelling of heat transfer, fluid flow, hydrocarbon generation and migration', *AAPG Bull.*, **74,** 309–335 (1990).
14. I. Faille, 'Modelisation bidimensionnelle de la genese et de la migration des hydrocarbures dans un bassin sedimentaire, *Ph.D. Thesis*, Universite Joseph Fourier, Grenoble, France, 1992.
15. F. Schneider, S. Wolf, I. Faille, T. Gallouet and W. Choueiri, 'Hydrocarbon migration in basin modelling: is the combined use of finite element and control volume possible', in M. A. Cristie, et al. (eds), *Proc. 3rd European Conf. of the Mathematics of Oil Recovery*, Delft University Press, The Netherlands, 1992, pp. 289–301.
16. J. Wendebourg, 'Migration of hydrocarbons', *Ph.D. Thesis*, Standford University, California, 1994.
17. I. Faille, Control volume method to model fluid flow on 2D irregular meshing, in D. Guerillot and O. Guillon (eds), *Proc. 2nd European Conf. on the Mathematics of Oil Recovery*, Arle 1990, Editions Technip, Paris, 1990, pp. 149–156.
18. H. P. Langtangen, 'Implicit finite element methods for two-phase flow in oil reservoirs', *Int. j. numer. Methods Fluids.*, **10,** 651–681 (1990).
19. R. E. Ewing and M. F. Wheeler, 'Galerkin methods for miscible displacement problems in porous media', *SIAM J. Numer. Anal.*, **17,** 351–365 (1980).
20. M. S. Espedal and R. E. Ewing, 'Characteristic Petrov-Galerkin subdomain methods for two-phase immiscible flow', *Comput. Methods Appl. Mech. Eng.*, 113–135 (1987).
21. V. Dalen, 'Simplified finite-element models for reservoir flow problems', *Soc. Pet. Eng. J.*, **19,** *Trans. AIME.* **267,** 333–343 (1979).
22. P. S. Huyakorn and G. F. Pinder, 'A new finite element technique for the solution of two-phase flow through porous media', *Adv. Water Resour.* **1,** 285–298 (1978).
23. S. Khataniar and J. P. Ekwere, 'A comparison of the finite-difference and the finite-element methods for simulating unstable displacements', *J. Pet. Sci. Eng.*, **5,** 205–218 (1991).
24. O. Langsrud, 'Simulation of two-phase flow by finite element method', *SPE Fourth Symp. Numerical Simulation of Reservoir Performance*, *SPE Paper 5725*, Los Angles, CA, 1976.
25. A. Spivak, H. S. Price and A. Settari, 'Solutions of the equations for multi-dimensional two-phase immiscible flow by variational methods', *SPE Fourth Symp. Numerical Simulation of Reservoir Performance*, *SPE Paper 5723*, Los Angles, CA, 1976.
26. G. Gottardi and D. Dall'Olio, 'A control-volume finite-element model for simulating oil–water reservoirs', *J. Pet. Sci. Eng.*, **8,** 29–41 (1992).
27. J. Lerche, *Basin Analysis. Quantitative Methods*, Vol. 1, Chapter 6, Academic Press, San Diego, 1990.
28. M. Wangen, 'Vertical migration of hydrocarbons modelled with fractional flow theory', *Geophys. J. Int.*, **115,** 109–131 (1993).
29. R. W. Lewis and B. A. Screfler, *The Finite Element Method in the Deformation and Consolidation of Porous Media*, Wiley, New York, 1987.
30. W. W. Rubey and M. K. Hubbert, 'Overtrust belt in geosynclinal area of western Wyoming in the light fluid-pressure hypothesis, 2: Role of fluid pressure in mechanicas of overtrust faulting', *Geol. Soc. Am. Bull.*, **70,** 167–205 (1959).
31. L. F. Athy, 'Density, porosity, and compaction of sedimentary rocks', *Bull. Amr. Assoc. Petrol. Geol.*, **14,** 1–24 (1930).
32. R. E. Gibson, R. L. Schiffman and K. W. Cargill, 'The theory of one-dimensional consolidation of saturated clays. II. Finite nonlinear consolidation of thick homogeneous layers', *Can. Geotech. J.*, **18,** 280–293.
33. J. B. Burland, 'On the compressibility and shear strength of natural clays', *Géotechnique*, **40,** 329–378 (1996).
34. K. Magara, *Geological Models of Petroleum Entrapment*, Elsevier Applied Science Publishers, London and New York, 1986.

35. B. P. Tissot and D. H. Welte, *Petroleum Formation and Occurrence*, Springer, Baslin, 1978.
36. W. R. Bryant, W. Hottman and P. Trabant, 'Permeability of unconsolidated marine sediments', Gulf of Mexico, *Mar. Geotechnol.*, **1,** 1–14 (1975).
37. C. R. Lewis and S. C. Rose, 'A theory relating high temperatures and over-pressures', *J. Petrol. Tech.*, **22,** 11–16 (1970).
38. L. W. Lake, *Enhanced Oil Recovery*, Prentice Hall, Englewood Cliffs, NJ. 1989.
39. R. C. Weast and M. J. Astle, *CRC Handbook of Chemistry and Physics*, 63rd edn, CRC Press Boca Raton, FL, 192.
40. E. N. Andrade and C. Da, 'The viscosity of liquids', *Nature* 309–310 (1930).
41. M. Wangen, 'Numerical simulation of thermal convection in compacting sedimentary basins', *Geophys. J. Int.*, **119,** 129–150 (1994).